Chemical Science

EDGE ARTICLE

View Article Online
View Journal | View Issue

Cite this: *Chem. Sci.*, 2014, **5**, 782

A dual approach to tuning the porosity of porous organic polymers: controlling the porogen size and supercritical CO_2 processing†

Ryan K. Totten, Laura L. Olenick, Ye-Seong Kim, Sanjiban Chakraborty, Mitchell H. Weston, Omar K. Farha,* Joseph T. Hupp* and SonBinh T. Nguyen*

Received 18th July 2013
Accepted 9th October 2013

DOI: 10.1039/c3sc52010b

www.rsc.org/chemicalscience

Porous organic polymers (POPs) with tunable pore volumes and surface areas can be made from a series of Sn^{IV}(porphyrins) functionalized with labile, bulky *trans*-diaxial ligands. Varying the ligand size allows for the tuning of the micropore volume while supercritical CO_2 processing resulted in excellent enhancements of the total pore volumes.

Introduction

Over the past decade, there has been a strong interest in porous organic polymers (POPs) due to their potential in applications such as catalysis,[1–9] gas storage,[10–16] and chemical separations.[4,17–20] The (co)polymerization of one (or more) rigid, multitopic organic building blocks can afford chemically and thermally stable microporous materials with a wide range of chemical functionalities, sizable internal surface areas, and substantial capacities for uptake of molecular guests.[13] Although POPs can be considered to be organic analogs of metal–organic frameworks (MOFs), their average pore volumes and surface areas tend to span a much smaller range.[2,21] Part of this limitation is due to the tendency of the planar aromatic monomers used in POP synthesis to stack *via* van der Waals interactions during the course of polymerization. Consequently, the majority of POPs are interpenetrating networks with relatively low total pore volumes and small pore diameters,[2,12] which limits the access and transport of molecular substrates in applications such as chemical and gas separations or catalysis.[2]

Thus far, strategies for controlling the pore properties and surface areas of POPs have involved the elaboration of organic building blocks/monomers,[4,16,22–25] the tuning of the reaction time and temperature,[3,26] and the choice of solvents.[8,27] Surprisingly, "templating", a strategy that is well-known in supramolecular chemistry to control distances between building blocks, has not been applied to the synthesis of POPs to generate large and accessible micropores. In theory, a molecular porogen (*i.e.*, a molecule that "generates" pores) that is attached to a building block, either covalently or through attractive van der Waals interactions, can occupy the empty space next to that building block during polymerization, preventing the formation of additional networks immediately proximal to the first one, and thus reduce interpenetration. The porogen can then be removed to reveal permanent micropores after network formation is complete. This strategy is akin to the use of block copolymers to generate mesopores in mesoporous silicas,[28,29] but would generate (sub)nanometer-sized micropores and ultramicropores, as shown recently in the synthesis of non-catenated IRMOFs.[30,31] Herein, we report the use of a porogen strategy to tune the surface areas and pore properties of a series of porphyrin POPs (PPOPs). We copolymerize the T_d-directing unit *tetrakis*(4-ethynylphenyl)methane with a series of Sn^{IV}(porphyrin) building blocks that have been functionalized with *trans*-diaxial ligands/porogens of differing sizes, all of which can be removed after POP formation to afford materials with tunable total pore volumes (0 to 1.42 $cm^3\ g^{-1}$) and microporosity (micropore volumes = 0 to 0.26 $cm^3\ g^{-1}$) after supercritical CO_2 processing.

Among the POPs that have been reported, those that are based on porphyrins have often been characterized by only moderate to low porosities (as measured by total pore volumes and surface areas).[2–4,32] This has been attributed to the tendency of the flat porphyrin rings to stack *via* noncovalent van der Waals interactions during polymerization, creating interpenetrated networks. We hypothesize that more porous materials could be made if the porphyrin monomers remained further apart during polymerization. Thus, we chose metalloporphyrin building blocks with sterically hindered axial ligands as a platform for evaluating the porogen strategy in POP synthesis. With a judicious choice of polymerization chemistry, the axial ligands can serve as convenient porogens that remain

Department of Chemistry and the International Institute for Nanotechnology, Northwestern University, 2145 Sheridan Road, Evanston, IL, 60208-3113, USA. E-mail: o-farha@northwestern.edu; j-hupp@northwestern.edu; stn@northwestern.edu

† Electronic supplementary information (ESI) available: Complete procedures for the synthesis of Sn-PPOP starting materials and characterization data (^1H and ^1H–^{13}C CP-MAS NMR, MALDI-ToF MS, UV-vis, elemental analysis); BET adsoprtion–desorption isotherms, pore size distribution profiles, solvent-exposed experiments, SEM images, and density measurements. See DOI: 10.1039/c3sc52010b

on the metal centers throughout the polymerization but can be removed after POP synthesis to yield permanent pores (Fig. 1). In addition, the ability to modulate the size of the axial ligands bound to the metal center should allow us to tune the pore properties of the resulting PPOPs. In particular, we selected as one of our monomers a class of Sn^{IV}(porphyrins) with *trans*-diaxial anionic ligands, which enable the attachment of two porogens to every metalloporphyrin unit.[33] For the initial evaluation, we chose ligands ranging from small to large in size, starting with hydroxide and chloride, then acetate, and finally a large (3,5-di-^{t}butyl)benzoate moiety. The effect of the porogen could then be evaluated across this series after work-up when all the axial ligands are exchanged away by the addition of excess acetic acid to yield a series of acetate-bound POPs (Scheme 1).

Results and discussion

For POP synthesis, we selected an acetylene trimerization strategy[22,34,35] given its short reaction times (~1.5 h) and the absence of any protonated reactants or side products that might exchange with the *trans*-diaxial ligands of the Sn^{IV}(porphyrin) monomers during polymerization. In the presence of $Co_2(CO)_8$, the copolymerization of the *tetrakis*(4-ethynylphenyl)methane monomer with either one of our four R_2-Sn^{IV}(porphyrin) monomers ($(HO)_2$-**Sn**, R = OH; $(Cl)_2$-**Sn**, R = Cl; $(AcO)_2$-**Sn**, R = acetate; $(^tBu_2BzO)_2$-**Sn**, R = 3,5-di-^{t}butyl benzoate; Scheme 1) proceeded smoothly to afford the desired POPs in quantitative yields as deep purple solids. The Sn-PPOPs were then treated with excess glacial acetic acid at 100 °C to remove any residual cobalt species. Assuming that all of the initial axial ligands are also exchanged, this should result in a series of *trans* di-acetate-substituted Sn-PPOPs with different surface and pore properties.

N_2 gas adsorption analyses clearly indicated that the nature of the initial ligand on the Sn^{IV}(porphyrin) monomer significantly affects the surface area and pore properties of the resulting Sn-PPOPs. For the $(HO)_2$-**Sn** and $(Cl)_2$-**Sn** monomers, the resulting Sn-PPOPs—**Sn-PPOP**↔$(OH)_2$ and **Sn-PPOP**↔$(Cl)_2$, respectively—are either non-porous (0 $cm^3\ g^{-1}$ total pore volume and 0 $m^2\ g^{-1}$ surface area for **Sn-PPOP**↔$(OH)_2$, Scheme 1) or have very low porosity (0.02 $cm^3\ g^{-1}$ total pore volume and 70 $m^2\ g^{-1}$ surface areas for **Sn-PPOP**↔$(Cl)_2$, Scheme 1). As expected, the small hydroxide and chloride ligands are not effective porogens and do not lead to materials with accessible pores or surface areas. Indeed, analysis by ^1H–^{13}C CP-MAS NMR spectroscopy shows only minimal exchange of acetate with the hydroxyl- and no exchange at all with the Cl-containing materials.

In contrast, **Sn-PPOP**↔$(AcO)_2$, the POP obtained from the di-acetate Sn^{IV}(porphyrin) ($(AcO)_2$-**Sn**) monomer, is quite porous (0.24 $cm^3\ g^{-1}$ total pore volume and 500 $m^2\ g^{-1}$ surface area; Table 1, entry 3a; see also Fig. 2), suggesting that the acetate ligands have enabled the formation of a reasonable number of micropores (9 and 12 Å; Table 1, entry 3a, see also Fig. 3). Presumably, the presence of the two medium acetate axial ligands is sufficient to disrupt the favorable van der Waals interactions between the porphyrin monomers and allow a microporous framework to be constructed.

The porogenic effect of the axial ligands becomes quite apparent in the case of the $(^tBu_2BzO)_2$-**Sn** monomer, where the presence of two large 3,5-di-^{t}butyl benzoate moieties on the Sn^{IV}(porphyrin) precursor significantly improves the porosity (0.36 $cm^3\ g^{-1}$ total pore volume and 700 $m^2\ g^{-1}$ surface area; Table 1, entry 4a; see also Fig. 2) of the resulting Sn-PPOP after the acetic acid wash. Remarkably, the total pore volume of this **Sn-PPOP**↔$(^tBu_2BzO)_2$ material is 50% more than that for the corresponding **Sn-PPOP**↔$(AcO)_2$ material and almost 20-fold that of **Sn-PPOP**↔$(Cl)_2$ (Table 1, *cf.* entries 2, 3a, and 4a). Not only has its total pore volume greatly increased, larger micropores (13 and 15 Å) and some mesopores (20 and 27 Å) have also formed (Table 1, entry 4a, see also Fig. 3). Coupled with the fact that **Sn-PPOP**↔$(^tBu_2BzO)_2$ has a very low total pore volume (0.02 $cm^3\ g^{-1}$) and surface area (50 $m^2\ g^{-1}$) prior to washing with acetic acid (Fig. S11 in the ESI†) and that we can observe the complete release of the di-^{t}butyl benzoate axial ligands after this wash (see Section S5 in the ESI†), it is clear that the porogen strategy is quite effective at enhancing the microporosity of this Sn^{IV}(porphyrin)-based POP.

Encouraged by the ability to tune the surface area and pore properties of Sn-PPOPs with a few simple carboxylate ligands, we reasoned that further enhancement would be possible if larger porogens/ligands were implemented. However, the use of such porogens in PPOP synthesis would increase the likelihood of them becoming trapped in the pores even after washing with acetate. Therefore, we incorporated acid-cleavable imine linkages into the carboxylate ligand i_2BzOH (3,5-*bis*[(3,5-di-*tert*-butyl)benzylideneamino]benzoic acid), which would be broken up into smaller fragments during the acetic acid work-up and thus become easier to remove from the pores. The complexation of i_2BzOH to $(HO)_2$-**Sn** proceeded smoothly to yield $(i_2BzO)_2$-**Sn** (Fig. 4) in good yield.

Interestingly, the copolymerization of $(i_2BzO)_2$-**Sn** with *tetrakis*(4-ethynylphenyl)methane only reached ~70% conversion,

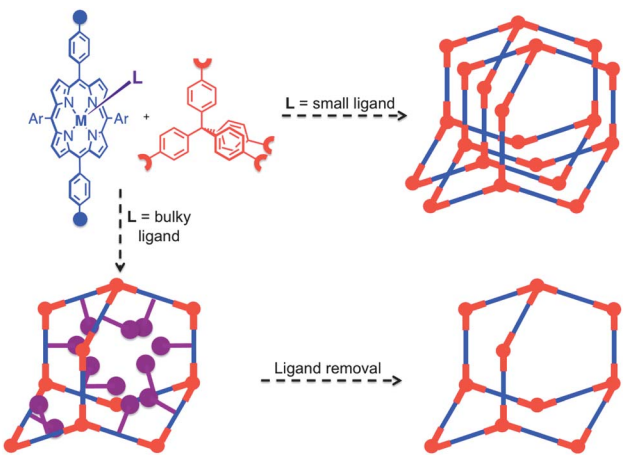

Fig. 1 An *idealized* schematic illustration of the porogen strategy in POP synthesis starting from a metalloporphyrin monomer functionalized with a bulky axial ligand.

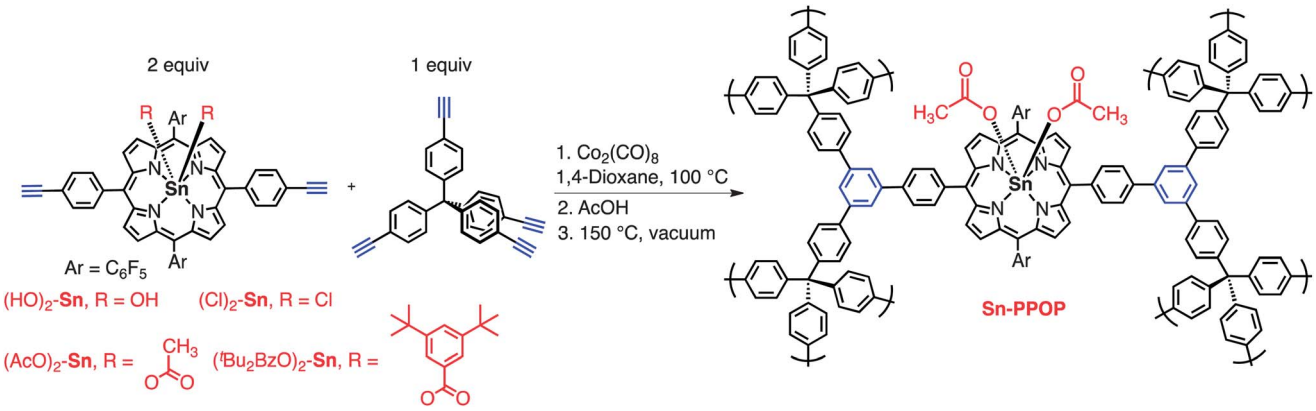

Scheme 1 Synthesis of Sn^{IV}(porphyrin)-based POPs using a cobalt-catalyzed acetylene trimerization strategy. For ease of viewing, the two acetate ligands on each Sn(porphyrin) unit are drawn with stereotopic wedges on the same side. However, they should be thought of as being axially ligated opposite each other. We note that the POPs shown above are idealized representations of a completely formed network. However, different substitution patterns (1,3,4 *vs.* 1,3,5) may be present as well as terminal olefins/dienes and unreacted acetylene groups due to incomplete polymerization. Indeed, solid-state ^1H–^{13}C CP-MAS NMR analysis suggested that these materials have significant numbers of olefin/diene groups (see Fig. S19 in the ESI†).

with a considerable amount of the porphyrin-containing oligomers still left in solution at the end (see Section S5 in the ESI†). Treatment of the resulting materials with "wet" acetic acid at 100 °C afforded the acetate-ligated polymer **Sn-PPOP**↔$(i_2BzO)_2$, with complete removal of the i_2BzOH porogen that was verified by GC analysis of the mother liquor of the acetic acid washings (see Section S5 in the ESI†). Surprisingly, BET analysis of this material revealed a total pore volume of only 0.29 $cm^3\ g^{-1}$ (total micropore volume = 0.21 $cm^3\ g^{-1}$) and a surface area of just 620 $m^2\ g^{-1}$, not significantly different from those of **Sn-PPOP**↔$(^tBu_2BzO)_2$ (Table 1, *cf.* entries 4a and 5a). Together with the lower yield mentioned above, these data suggested that the ability of $(i_2BzO)_2$-**Sn** to completely copolymerize with *tetrakis*(4-ethynylphenyl)methane could have been hindered by the very large i_2BzOH porogens, as they may block additional co-monomer units from reacting with all the terminal acetylenes of the particular $(i_2BzO)_2$-**Sn** monomer. The result is an incompletely formed network that may not be as rigid and thus may be more prone to pore-collapse. This incomplete-polymerization hypothesis is supported by the solid-state ^1H–^{13}C CP-MAS NMR spectrum of **Sn-PPOP**↔$(i_2BzO)_2$, which shows a significant amount of internal olefin/diene groups, much more than that present in the corresponding spectrum for **Sn-PPOP**↔$(^tBu_2BzO)_2$ (see Fig. S19 in the

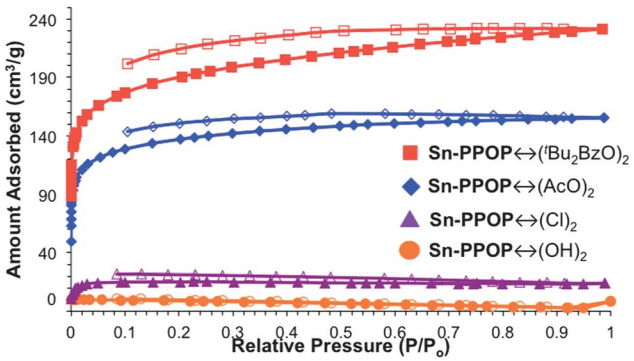

Fig. 2 N_2 isotherms measured at 77 K for **Sn-PPOP**↔$(OH)_2$ (orange circles), **Sn-PPOP**↔$(Cl)_2$ (purple triangles), **Sn-PPOP**↔$(AcO)_2$ (blue diamonds), and **Sn-PPOP**↔$(^tBu_2BzO)_2$ (red squares). Closed symbols, adsorption; open symbols, desorption.

Table 1 Pore and surface properties of Sn^{IV}(porphyrin)-based POPs

Entry	POP[a]	Dominant pore diameter (Å)	Total pore volume ($cm^3\ g^{-1}$)	Total micropore volume ($cm^3\ g^{-1}$)	Bulk density ($g\ cm^{-3}$)	BET surface area ($m^2\ g^{-1}$)
1a	**Sn-PPOP**↔$(OH)_2$	0	0	0	—	0
1b	^{scp}**Sn-PPOP**↔$(OH)_2$	12, 15	1.02	0.17	0.70	800
2	**Sn-PPOP**↔$(Cl)_2$	9	0.02	0.02	—	70
3a	**Sn-PPOP**↔$(AcO)_2$	9, 12	0.24	0.19	—	500
3b	^{scp}**Sn-PPOP**↔$(AcO)_2$	13, 15	1.13	0.20	0.64	880
4a	**Sn-PPOP**↔$(^tBu_2BzO)_2$	13, 15, 20, 27	0.36	0.26	—	700
4b	^{scp}**Sn-PPOP**↔$(^tBu_2BzO)_2$	10, 12, 15, 27	1.42	0.23	0.49	1100
5a	**Sn-PPOP**↔$(i_2BzO)_2$	10, 12, 15, 20, 27	0.29	0.21	—	620
5b	^{scp}**Sn-PPOP**↔$(i_2BzO)_2$	12, 15, 27	1.27	0.24	0.54	1000

[a] The notation **Sn-PPOP**↔$(ligand)_2$ was used to indicate that this Sn-PPOP material was derived from the corresponding $(ligand)_2$**Sn** comonomer but was subjected to an acetic acid work-up. For **Sn-PPOP**↔$(Cl)_2$, the axial ligands are most likely chlorides. For **Sn-PPOP**↔$(OH)_2$, the axial ligands are probably a mixture of acetates and hydroxyls. For **Sn-PPOP**↔$(AcO)_2$, **Sn-PPOP**↔$(^tBu_2BzO)_2$, and **Sn-PPOP**↔$(i_2BzO)_2$, the axial ligands are most likely acetates. See further discussion at the beginning of the Results and discussion section.

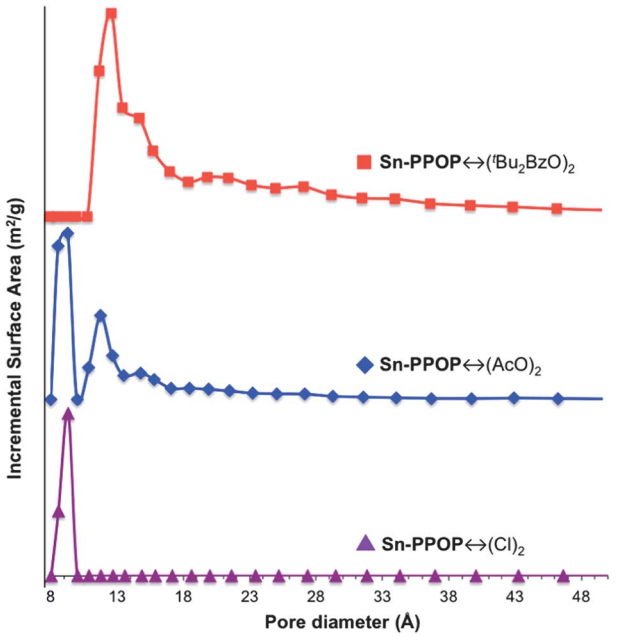

Fig. 3 BET-derived pore size distribution plots for **Sn-PPOP**↔$(Cl)_2$ (purple triangles), **Sn-PPOP**↔$(AcO)_2$ (blue diamonds), and **Sn-PPOP**↔$(^tBu_2BzO)_2$ (red squares).

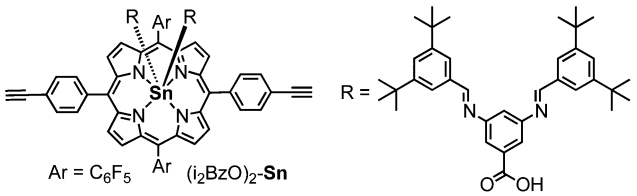

Fig. 4 Structure of $(i_2BzO)_2$-**Sn** with cleavable imine-based ligands. For ease of viewing, the two i_2BzO ligands on the Sn(porphyrin) unit are drawn with stereotopic wedges on the same side. However, they should be thought of as being axially ligated opposite each other.

ESI†). Further reinforcing this notion is the pore size distribution (PSD) profile for **Sn-PPOP**↔$(i_2BzO)_2$, which shows a significant amount of mesoporosity compared to the profiles for **Sn-PPOP**↔$(OH)_2$, **Sn-PPOP**↔$(Cl)_2$, and **Sn-PPOP**↔$(AcO)_2$. Indeed, the solid-state ^1H–^{13}C CP-MAS NMR spectrum and PSD profile of **Sn-PPOP**↔$(i_2BzO)_2$ have many similar features to those of **Sn-PPOP**↔$(^tBu_2BzO)_2$, suggesting that there is an upper limit to the size of the axial ligand that could be used in the porogen strategy such that complete polymerization can be achieved and yields are not compromised.

Our data thus far clearly indicates that the incorporation of bulky axial ligands on Sn^{IV}(porphyrin) monomers can significantly increase the microporosity of the resulting Sn-PPOPs after acetate exchange. However, for many catalysis and storage applications, the facile accessibility of these pores is also very important.[36–38] As shown for MOFs,[39,40] accessibility to the pores of microporous materials can be significantly diminished by undesirable particle aggregation or pore collapse, which occurs after thermal activation. The surface tension and capillary forces of such a process (*i.e.*, removing the trapped solvent too quickly), cause the collapse of large "interparticle" pores (*i.e.*, the void volume in between the polymer particles), and hence limit accessibility to the internal micropore environment. Suspecting that the pore volumes and surface areas of our Sn-PPOP materials could be improved if these large pores were available, we decided to process the PPOP materials using supercritical CO_2 processing. Recent work in our group has demonstrated that supercritical CO_2 processing of Al(porphyrin)-based POPs significantly increases the accessibility of Al^{III} sites to a solution-phase reactant (a phosphate triester), thereby enhancing the catalytic effectiveness of this material in the methanolytic degradation of the phosphate triester.[41] In addition, earlier work with crystalline MOFs revealed that supercritical processing is effective for preventing pore collapse.[39,42]

To avoid potential pore collapse from thermal activation, both the as-synthesized **Sn-PPOP**↔$(^tBu_2BzO)_2$ and the **Sn-PPOP**↔$(i_2BzO)_2$ materials were solvent-exchanged with absolute ethanol from their solvent-wetted, gel-like states and then processed with supercritical CO_2.[39] As expected, the supercritical CO_2-processed ^{scp}**Sn-PPOP**↔$(^tBu_2BzO)_2$ displays a significantly higher surface area (1100 $m^2\ g^{-1}$) compared to the thermally activated sample (700 $m^2\ g^{-1}$) (Table 1, *cf.* entries 4a and 4b). Additionally, ^{scp}**Sn-PPOP**↔$(^tBu_2BzO)_2$ now exhibits a type II adsorption isotherm with a hysteretic desorption branch, indicating a significant presence of mesoporosity (Fig. 5a). Most impressive however, is the 300% gain in the total pore volume (from 0.36 to 1.42 $cm^3\ g^{-1}$). This dramatic increase is reflected in the pore size distribution, which shows dominant pore sizes

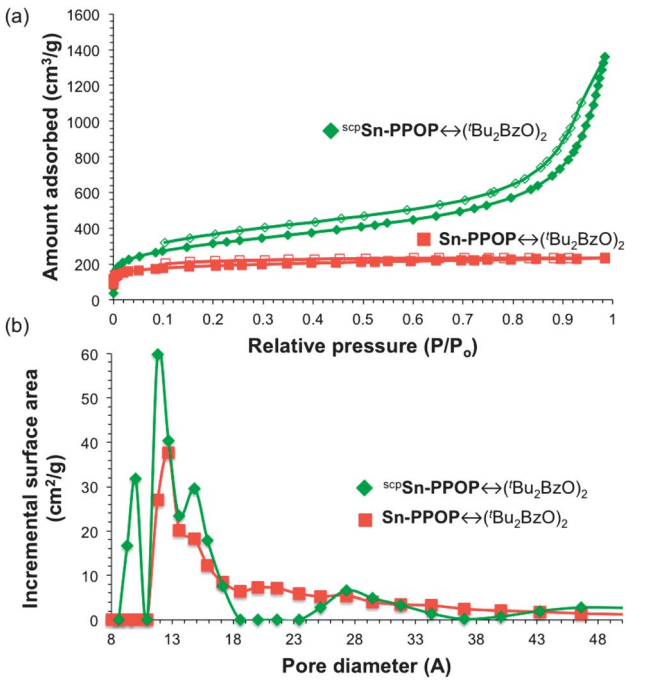

Fig. 5 (a) N_2 isotherms measured at 77 K for **Sn-PPOP**↔$(^tBu_2BzO)_2$ (red squares) and ^{scp}**Sn-PPOP**↔$(^tBu_2BzO)_2$ (green diamonds). Closed symbols, adsorption; open symbols, desorption. (b) BET-derived pore size distribution plots for **Sn-PPOP**↔$(^tBu_2BzO)_2$ (red squares) and ^{scp}**Sn-PPOP**↔$(^tBu_2BzO)_2$ (green diamonds).

of 10, 12, and 15 Å as well as a populated mesoporous region centered at 27 Å (Fig. 5b). Interestingly, the total micropore volume remains relatively unchanged from the thermally activated sample to the supercritical CO_2-processed one (0.26 *vs.* 0.23 $cm^3\ g^{-1}$), demonstrating that the large gain in total pore volume is due exclusively to the presence of larger "interparticle" pores that are preserved in ^{scp}**Sn-PPOP↔**$(^tBu_2BzO)_2$.

Similarly, the supercritical CO_2-processed ^{scp}**Sn-PPOP↔**$(i_2BzO)_2$ sample displays an enhanced total pore volume (1.27 $cm^3\ g^{-1}$) and surface area (1000 $m^2\ g^{-1}$) compared to those of the thermally activated sample (Table 1, *cf.* entries 5a and 5b). As in the case for ^{scp}**Sn-PPOP↔**$(^tBu_2BzO)_2$, the total micropore volumes for the thermally activated and supercritical CO_2-processed samples are similar (0.21 *vs.* 0.24 $cm^3\ g^{-1}$). Together, all of these data suggest that tuning the porogen size has the largest effect on the microporosity of the resulting POPs while supercritical processing can be used to preserve larger pores.

As a comparison, the non-porous material **Sn-PPOP↔**$(OH)_2$ was also re-synthesized and processed with supercritical CO_2. Interestingly, the total pore volume of the supercritical CO_2-processed sample, ^{scp}**Sn-PPOP↔**$(OH)_2$, was greatly improved from that of the thermally activated sample, **Sn-PPOP↔**$(OH)_2$ (1.02 *vs.* 0 $cm^3\ g^{-1}$; Table 1, *cf.* entries 1a and 1b). The BET surface area was similarly improved (800 *vs.* 0 $m^2\ g^{-1}$; Table 1, *cf.* entries 1a and 1b). While this may appear surprising at first, the bulk density of ^{scp}**Sn-PPOP↔**$(OH)_2$ (0.7 g cm^{-3}) is still higher than those of ^{scp}**Sn-PPOP↔**$(AcO)_2$, ^{scp}**Sn-PPOP↔**$(^tBu_2BzO)_2$ and ^{scp}**Sn-PPOP↔**$(i_2BzO)_2$ (0.64, 0.49, and 0.54 g cm^{-3}, respectively, see Section S12 in the ESI†), suggesting that there is a higher degree of interpenetration in ^{scp}**Sn-PPOP↔**$(OH)_2$ than in the remaining three materials. As such, the significant increase in the surface area and total pore volume in ^{scp}**Sn-PPOP↔**$(OH)_2$ can only be attributed to the decrease in aggregation of the POP particles, which allows the N_2 "probe molecules" to access the large "interparticle" pores as well as micropores that were previously inaccessible in the thermally activated sample (total micropore volume = 0.17 $cm^3\ g^{-1}$). This is supported by the similar gains in non-micropore volumes[43] for ^{scp}**Sn-PPOP↔**$(OH)_2$ and ^{scp}**Sn-PPOP↔**$(AcO)_2$ upon supercritical CO_2 activation (0.85 and 0.88 $cm^3\ g^{-1}$, respectively).

Conclusions

In summary, we have demonstrated that the total pore volumes and microporosity of Sn^{IV}(porphyrin)-based POPs can be tuned by incorporating Sn^{IV}(porphyrin) monomers possessing axial ligands of differing sizes into an all-organic porous network. The porogens can be easily removed after the formation of the POP network to reveal permanent micropores and mesopores. While a direct correlation exists between the size of the porogen, the total micropore volumes and the pore diameters, there is a limit to the size of the porogen that can be used, as one that is too large will cause low polymerization yields and incomplete network formation. Finally, the total pore volumes of POPs can be greatly enhanced through supercritical CO_2 processing of the Sn-PPOPs. In contrast to thermal activation, supercritical CO_2 processing preserves the as-synthesized Sn-PPOPs in their "expanded" state, retaining the void volumes in between the polymer networks and dramatically increasing pore accessibility. As POPs continue to find more applications in gas storage, separations, and heterogeneous catalysis, a synergistic combination of the porogen strategy and supercritical CO_2 processing could be tremendously useful in obtaining POPs with high surface areas and large, accessible pores.

Acknowledgements

Financial support for this work is provided by DTRA (agreement HDTRA1-10-1-0023). Instruments in the Northwestern University Integrated Molecular Structure Education and Research Center (IMSERC) were purchased with grants from NSF-NSEC, NSF-MRSEC, Keck Foundation, the state of Illinois, and Northwestern University.

Notes and references

1 J.-X. Jiang, C. Wang, A. Laybourn, T. Hasell, R. Clowes, Y. Z. Khimyak, J. Xiao, S. J. Higgins, D. J. Adams and A. I. Cooper, *Angew. Chem., Int. Ed.*, 2011, **50**, 1072–1075.
2 P. Kaur, J. T. Hupp and S. T. Nguyen, *ACS Catal.*, 2011, **1**, 819–835.
3 H. J. Mackintosh, P. M. Budd and N. B. McKeown, *J. Mater. Chem.*, 2008, **18**, 573–578.
4 N. B. McKeown and P. M. Budd, *Chem. Soc. Rev.*, 2006, **35**, 675–683.
5 A. M. Shultz, O. K. Farha, J. T. Hupp and S. T. Nguyen, *Chem. Sci.*, 2011, **2**, 686–689.
6 Z. Xie, C. Wang, K. E. deKrafft and W. Lin, *J. Am. Chem. Soc.*, 2011, **133**, 2056–2059.
7 Y. Zhang and S. N. Riduan, *Chem. Soc. Rev.*, 2012, **41**, 2083–2094.
8 L. Chen, Y. Yang and D. Jiang, *J. Am. Chem. Soc.*, 2010, **132**, 9138–9143.
9 L. Chen, Y. Yang, Z. Guo and D. Jiang, *Adv. Mater.*, 2011, **23**, 3149–3154.
10 T. Ben, H. Ren, S. Ma, D. Cao, J. Lan, X. Jing, W. Wang, J. Xu, F. Deng, J. M. Simmons, S. Qiu and G. Zhu, *Angew. Chem., Int. Ed.*, 2009, **48**, 9457–9460.
11 Q. Chen, M. Luo, P. Hammershøj, D. Zhou, Y. Han, B. W. Laursen, C.-G. Yan and B.-H. Han, *J. Am. Chem. Soc.*, 2012, **134**, 6084–6087.
12 A. I. Cooper, *Adv. Mater.*, 2009, **21**, 1291–1295.
13 B. G. Hauser, O. K. Farha, J. Exley and J. T. Hupp, *Chem. Mater.*, 2012, **25**, 12–16.
14 M. G. Rabbani and H. M. El-Kaderi, *Chem. Mater.*, 2011, **23**, 1650–1653.
15 J. Weber and A. Thomas, *J. Am. Chem. Soc.*, 2008, **130**, 6334–6335.
16 D. Yuan, W. Lu, D. Zhao and H.-C. Zhou, *Adv. Mater.*, 2011, **23**, 3723–3725.
17 O. K. Farha, A. M. Spokoyny, B. G. Hauser, Y.-S. Bae, S. E. Brown, R. Q. Snurr, C. A. Mirkin and J. T. Hupp, *Chem. Mater.*, 2009, **21**, 3033–3035.

18 G. W. Peterson, O. K. Farha, B. Schindler, P. Jones, J. Mahle and J. T. Hupp, *J. Porous Mater.*, 2012, **19**, 261–266.
19 M. G. Rabbani and H. M. El-Kaderi, *Chem. Mater.*, 2012, **24**, 1511–1517.
20 X. Liu, Y. Xu, Z. Guo, A. Nagai and D. Jiang, *Chem. Commun.*, 2013, **49**, 3233–3235.
21 R. Dawson, A. I. Cooper and D. J. Adams, *Prog. Polym. Sci.*, 2012, **37**, 530–563.
22 R. K. Totten, M. H. Weston, J. K. Park, O. K. Farha, J. T. Hupp and S. T. Nguyen, *ACS Catal.*, 2013, **3**, 1454–1459.
23 J.-X. Jiang, F. Su, A. Trewin, C. D. Wood, H. Niu, J. T. A. Jones, Y. Z. Khimyak and A. I. Cooper, *J. Am. Chem. Soc.*, 2008, **130**, 7710–7720.
24 R. Dawson, D. J. Adams and A. I. Cooper, *Chem. Sci.*, 2011, **2**, 1173–1177.
25 L. Ma, M. M. Wanderley and W. Lin, *ACS Catal.*, 2011, **1**, 691–697.
26 P. Pandey, O. K. Farha, A. M. Spokoyny, C. A. Mirkin, M. G. Kanatzidis, J. T. Hupp and S. T. Nguyen, *J. Mater. Chem.*, 2011, **21**, 1700–1703.
27 P. Pandey, A. P. Katsoulidis, I. Eryazici, Y. Wu, M. G. Kanatzidis and S. T. Nguyen, *Chem. Mater.*, 2010, **22**, 4974–4979.
28 S. A. Davis, M. Breulmann, K. H. Rhodes, B. Zhang and S. Mann, *Chem. Mater.*, 2001, **13**, 3218–3226.
29 P. Innocenzi, L. Malfatti and G. J. A. A. Soler-Illia, *Chem. Mater.*, 2011, **23**, 2501–2509.
30 R. K. Deshpande, J. L. Minnaar and S. G. Telfer, *Angew. Chem., Int. Ed.*, 2010, **49**, 4598–4602.
31 D. J. Lun, G. I. N. Waterhouse and S. G. Telfer, *J. Am. Chem. Soc.*, 2011, **133**, 5806–5809.
32 A. Modak, M. Nandi, J. Mondal and A. Bhaumik, *Chem. Commun.*, 2012, **48**, 248–250.
33 D. P. Arnold and J. Blok, *Coord. Chem. Rev.*, 2004, **248**, 299–319.
34 M. H. Weston, O. K. Farha, B. G. Hauser, J. T. Hupp and S. T. Nguyen, *Chem. Mater.*, 2012, **24**, 1292–1296.
35 M. H. Weston, G. W. Peterson, M. A. Browe, P. Jones, O. K. Farha, J. T. Hupp and S. T. Nguyen, *Chem. Commun.*, 2013, **49**, 2995–2997.
36 M. Hartmann, *Angew. Chem., Int. Ed.*, 2004, **43**, 5880–5882.
37 H. Chen, J. Wydra, X. Zhang, P.-S. Lee, Z. Wang, W. Fan and M. Tsapatsis, *J. Am. Chem. Soc.*, 2011, **133**, 12390–12393.
38 T. M. McDonald, W. R. Lee, J. A. Mason, B. M. Wiers, C. S. Hong and J. R. Long, *J. Am. Chem. Soc.*, 2012, **134**, 7056–7065.
39 A. P. Nelson, O. K. Farha, K. L. Mulfort and J. T. Hupp, *J. Am. Chem. Soc.*, 2008, **131**, 458–460.
40 C.-S. Tsao, C.-Y. Chen, T.-Y. Chung, C.-J. Su, C.-H. Su, H.-L. Chen, U. S. Jeng, M.-S. Yu, P.-Y. Liao, K.-F. Lin and Y.-R. Tzeng, *J. Phys. Chem. C*, 2010, **114**, 7014–7020.
41 R. K. Totten, Y.-S. Kim, M. H. Weston, O. K. Farha, J. T. Hupp and S. T. Nguyen, *J. Am. Chem. Soc.*, 2013, **135**, 11720–11723. We note that supercritical CO_2-processed Al(porphyrin) POPs irreversibly shrink when exposed to organic solvents and allowed to dry, thereby losing the large interparticle micro- and mesopores originally gained *via* supercritical CO_2 processing.
42 O. K. Farha and J. T. Hupp, *Acc. Chem. Res.*, 2010, **43**, 1166–1175.
43 Gain in non-micropore volumes upon supercritical CO_2 activation = (Total pore volume − total micropore volume)$|_{\text{supercritically processed materials}}$ − (Total pore volume − total micropore volume)$|_{\text{thermally activated materials}}$.